Supporting Information: Cavity control of Excitons in two dimensional Materials

Simone Latini,*,†,§ Enrico Ronca,*,†,§ Umberto De Giovannini,†,‡

Hannes Hübener,† and Angel Rubio*,†,¶

†*Max Planck Institute for the Structure and Dynamics of Matter, Luruper Chaussee 149, 22761 Hamburg, Germany.*

Center for Free-Electron Laser Science and Department of Physics, University of Hamburg, Luruper Chaussee 149, 22761 Hamburg, Germany

‡*Dipartimento di Fisica e Chimica, Universitá degli Studi di Palermo, Via Archirafi 36, I-90123, Palermo, Italy*

¶*Center for Computational Quantum Physics (CCQ), The Flatiron Institute, 162 Fifth avenue, New York NY 10010.*

§*Contributed equally to this work*

E-mail: simone.latini@mpsd.mpg.de; enrico.ronca@mpsd.mpg.de; angel.rubio@mpsd.mpg.de

QED-BSE Computational Details

All of the ab-initio calculations for the electronic problem in this work are performed with the GPAW code.[1,2] The single particle energies and wavefunctions, together with the momentum matrix elements $\langle \phi_{i\mathbf{k}} | \hat{e} \cdot \hat{p} | \phi_{j\mathbf{k}} \rangle$ are calculated within density functional theory with the LDA exchange correlation functional on a plane-wave basis. The LDA calculations for the monolayers TMDs were performed using a plane wave basis set with a cut off energy of 500 eV and 60×60 k-point grids.

We calculate the excitonic wavefunctions used in the QED Hamiltonian by solving the BSE considering only electron-hole pairs formed between the top valence and bottom conduction band. We take a cut-off energy of 150 eV for the evaluation of the screened interaction, which is calculated within the RPA on LDA energies and wavefunctions. A scissor operator based on the G_0W_0 calculations is applied for a better description of the electronic gap, see Tab. S1 for specific values. Spin-orbit effects are included post BSE solution by including two equivalent spin-orthogonal (A and B) excitonic series. Spin-orbit splitting values are reported in Tab. S1. The Brillouin zone sampling for BSE and G_0W_0 calculations is done on a 60×60 k-point-mesh.

Table S1: GW band gap and SOC splittings for different TMDs. All values are extracted from the C2DB two-dimensional materials database[3]

TMD	GW gap (eV)	SOC split (eV)
MoS_2	2.53	0.15
$MoSe_2$	2.14	0.17
WS_2	2.60	0.37
WSe_2	2.21	0.40

Finally, in the QED Hamiltonian 18 excitonic states (up to the $3s$), a single photon mode with photon number states up to $\gamma = 3$ are included. These values have been chosen as result of convergence tests on the matter polarizability spectra in the energy region and $\tilde{A}_0$ values investigated here. Convergence with respect to the number of modes is discussed in more details in the following section. Exciton-polariton dispersions for MoS_2, WS_2, $MoSe_2$ and WSe_2 are shown in Fig. S1

QED-BSE Multi-mode Calculations

To avoid unnecessary complications, in the main text we only treated a single cavity mode. Eq. (1) of the main text can be directly generalized to the case of multiple modes, in formulas:

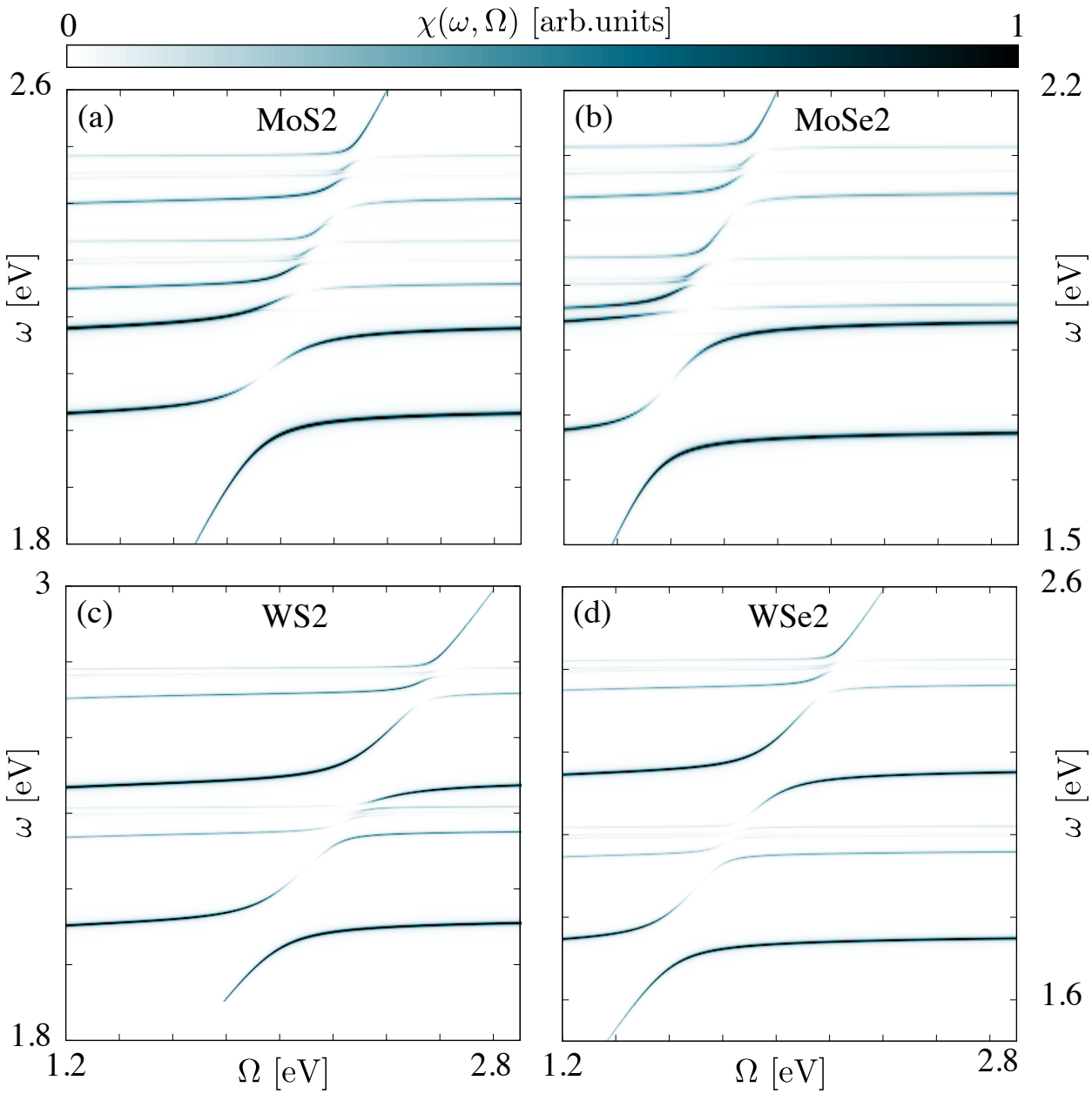

Figure S1: Exciton polariton dispersion of different TMDs with a coupling constant of $\tilde{A}_0$=0.08 a.u..

$$\begin{aligned}\hat{H}_{\mathrm{QED}} =& \hat{H}_{\mathrm{el}} + \sum_{\mathbf{q}\sigma} \Omega_q \hat{a}^\dagger_{\mathbf{q}\sigma} \hat{a}_{\mathbf{q}\sigma} + \\ & \frac{N_{\mathrm{el}}}{2} \sum_{\mathbf{q}\sigma} A^2_{0\mathbf{q}\sigma} \left| (u^*_{\mathbf{q}\sigma} \hat{a}^\dagger_{\mathbf{q}\sigma} + u_{\mathbf{q}\sigma} \hat{a}_{\mathbf{q}\sigma}) \right|^2 + \\ & \sum_{\mathbf{q}\sigma} A_{0\mathbf{q}\sigma} \sum_{ij\mathbf{k}\mathbf{k}'} \left(\langle \phi_{i\mathbf{k}} | u^*_{\mathbf{q}\sigma} \hat{p}_\sigma | \phi_{j\mathbf{k}'} \rangle \hat{d}^\dagger_{i\mathbf{k}} \hat{d}_{j\mathbf{k}'} \hat{a}^\dagger_{\mathbf{q}\sigma} + h.c. \right),\end{aligned} \tag{1}$$

where $\mathbf{q}$ is the photon momentum, σ the x, y, z index and $u_{\mathbf{q}\sigma}$ the photon polarization vectors. In a quasi-2D cavity the latter are given by:

$$\begin{aligned} u_{\mathbf{q}x} =& u_{\mathbf{q}y} = e^{i\mathbf{q}_\parallel \cdot \mathbf{r}_\parallel} i \sin(q_\perp z), \\ & u_{\mathbf{q}z} = e^{i\mathbf{q}_\parallel \cdot \mathbf{r}_\parallel} \cos(q_\perp z). \end{aligned} \tag{2}$$

In our work the relevant quantization dimension is the out-of-plane one and we only consider photon modes for which $\mathbf{q}_\parallel = 0$. We then assume that the active 2D crystal has an infinitesimal thickness and it is placed at the center of the cavity, namely $z = L_\perp/2$. Given the isotropy of TMDs monolayers, we can choose the in plane polarization to be in the y-direction, without any loss of generality. In such a setting and because 2D excitons can only couple to in-plane electric fields we consider only polarization of the kind $u_{\mathbf{q}y} = i \sin(q_\perp L_\perp/2)$ and of these only the odd modes are non-zero, i.e. $q_\perp = \frac{\pi\alpha}{L_\perp}$ with $\alpha = 1, 3, 5, ...$ With the restriction of the modes just described, the long wavelenght approximation can be still applied and we can simplify the Hamiltonian in Eq. 1 as:

$$\begin{aligned} \hat{H}_{\mathrm{QED}} =& \hat{H}_{\mathrm{el}} + \sum_\alpha \Omega_\alpha \hat{a}^\dagger_\alpha \hat{a}_\alpha + \frac{N_{\mathrm{el}}}{2} \sum_\alpha A^2_{0\alpha} \left|(\hat{a}^\dagger_\alpha + \hat{a}_\alpha)\right|^2 + \\ & \sum_\alpha A_{0\alpha} \sum_{ij\mathbf{k}} \left(\langle \phi_{i\mathbf{k}} | \hat{e} \cdot \hat{p} | \phi_{j\mathbf{k}} \rangle \hat{d}^\dagger_{i\mathbf{k}} \hat{d}_{j\mathbf{k}} \hat{a}^\dagger_\alpha + h.c. \right), \end{aligned} \tag{3}$$

with $\Omega_\alpha = \alpha\pi c/L_\perp$ and $A_{0\alpha} = 1/\sqrt{2\pi c S}\sqrt{\alpha}$.

Following the procedure we used for the single mode case, we project the Hamiltonian above onto the product state basis $|\Psi^{\mathrm{exc}}_n\rangle \otimes |\gamma^{\alpha=1}\rangle \otimes |\gamma^{\alpha=3}\rangle \otimes \cdots$, where $|\gamma^\alpha\rangle$ are the eigenfunctions of the photonic harmonic oscillator associated with the different modes. The Hamiltonian can be then diagonalized and the resulting polaritonic states and energy can be used for calculating the optical response as in Eq. (5) of the main text. Calculations for MoS_2 with up to $\alpha = 9$ are reported in Fig. S2. Within the Ω range considered in the main text the multi-mode calculation is in quantitative agreement with the single-mode one. However including more modes allows us to explore smaller values of Ω, where polaritonic

effects due to the higher modes take place.

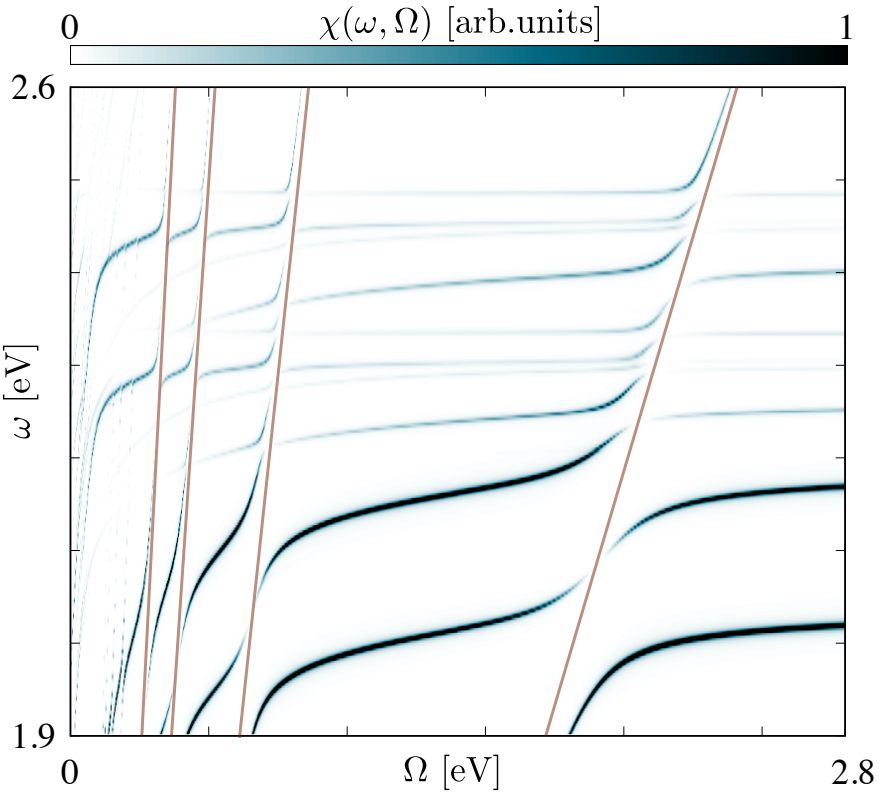

Figure S2: Exciton-polariton spectra of MoS_2 in a cavity as a function of cavity mode frequency Ω obtained with a multi-mode model with $\alpha = 9$ modes and a coupling strength of $\tilde{A}_0 = 0.08$ a.u..

Photon response

Equivalently to eq. 5 in the main text, a response function for photons can be also formulated:

$$\chi^{phot}(\omega, \Omega) = \sum_I \frac{(\tilde{\mathcal{M}}^{\rm pol}_{I0})^* \tilde{\mathcal{M}}^{\rm pol}_{I0}}{\omega - E^{\rm pol}_I(\Omega) + E^{\rm pol}_0(\Omega) + i\eta}. \tag{4}$$

In this case, the matrix elements are defined as $\tilde{\mathcal{M}}^{\rm pol}_{IJ} = \langle \Psi^{\rm pol}_I | \hat{a}^\dagger | \Psi^{\rm pol}_J \rangle = \sum_{n\gamma\theta} C^{I*}_{n\gamma} C^J_{m\theta} \mathcal{M}^{\rm phot}_{\gamma\theta}$ where $\mathcal{M}^{\rm phot}_{\gamma\theta} = \langle \gamma | \hat{a}^\dagger | \theta \rangle$. Such a quantity represents the photonic counterpart of the matter polarizability and it is of relevance for experiments where the photons are probed. The comparison between the matter and photon polarizabilities of MoS_2 for the stronger coupling values is presented in Fig. S3. The two response functions provide complementary informa-

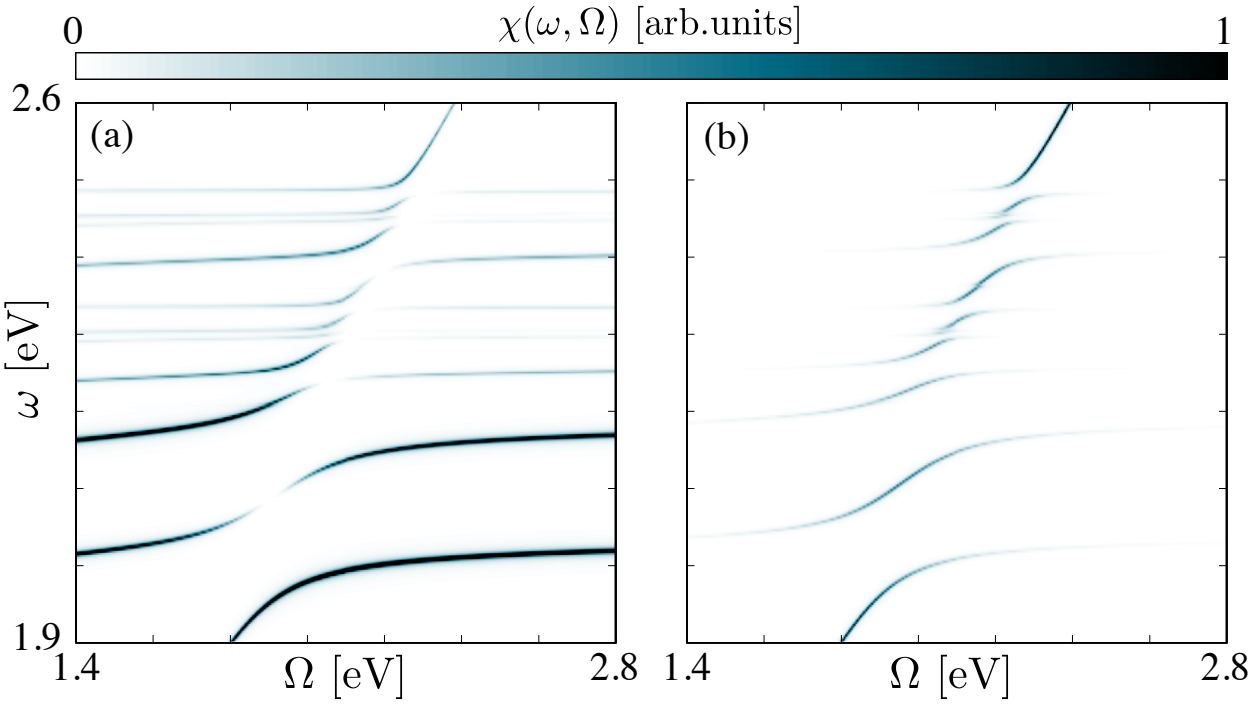

Figure S3: Comparison between (a) matter and (b) photon polarizabilitues for MoS_2 for a coupling value $\tilde{A}_0 = 0.08$ a.u..

tion on the polaritonic response, with the photonic response function showing a feature-rich matter-dressing of the bare photon line.

MW Method and Computational Details

In the MW model, the exciton is treated as a hydrogen atom, where the electron and the hole interact via a screened Coulomb interaction, described by the Schrödinger equation[4]

$$\left[-\frac{\nabla^2}{2\mu} - W(\mathbf{r})\right] F^n(\mathbf{r}) = E^n_{b,\mathrm{exc}} F^n(\mathbf{r}). \tag{5}$$

with μ the exciton effective mass and the screened Coulomb interaction

$$W(\mathbf{r}) = \frac{1}{4\alpha}\left[H_0(x) - N_0(x)\right]_{x=r/2\pi\alpha}, \tag{6}$$

where H_0 and N_0 are the Struve and Neumann functions and α is the crystal polarizability. By solving Eq. (5), we obtain exciton binding energies ($E^n_{b,\mathrm{exc}} = E_{\mathrm{gap}} - E^n_{\mathrm{exc}}$) and real space excitonic functions $F^n(\mathbf{r})$. Within the MW model, the latter represent the Fourier transforms of the envelope functions $A^n_{\mathbf{k}}$, i.e.

$$F^n(\mathbf{r}) = \frac{1}{N_k} \sum_{\mathbf{k}} A^n_{\mathbf{k}} e^{i\mathbf{k}\cdot\mathbf{r}}. \tag{7}$$

We stress that the coefficients $A^n_{\mathbf{k}}$ used in this section are the MW approximation to those defined above for BSE. An extensive discussion on the MW approach, the related computational advantages and how it can be derived as an approximation of the BSE can be found in Ref.[4]

Borrowing the assumptions of the MW model, in particular that the excitons are extremely localized at certain points in the Brillouin zone, the K-points for TMDs, we assume that the valence-conduction momentum matrix element is constant, and simplify Eq. (3) of the main text to:

$$\mathcal{M}^{\mathrm{exc}}_{0n} = \langle \phi_{\mathrm{vK}} | \hat{e} \cdot \hat{p} | \phi_{\mathrm{cK}} \rangle F^n(\mathbf{r} = 0). \tag{8}$$

This shows that whether an exciton is bright or dark, is determined by the value of its real space wavefunction at the origin. This explains why only s-like excitons are bright. Simplifications can also be done for Eq. (4) of the main text by noting that, for parabolic conduction and valence bands, $\langle \phi_{c/v\mathbf{k}} | \hat{e} \cdot \hat{p} | \phi_{c/v\mathbf{k}} \rangle = \pm k/m_{\mathrm{e/h}}$ giving

$$\mathcal{M}^{\mathrm{exc}}_{mn} = \left[\frac{1}{m_h} + \frac{1}{m_e} \right] \sum_{\mathbf{k}} A^{m*}_{\mathbf{k}} A^n_{\mathbf{k}} \; \hat{e} \cdot \mathbf{k}. \tag{9}$$

The sum in the RHS can be expressed as the expectation value of the dipole operator, $\sum_{\mathbf{k}} A^{m*}_{\mathbf{k}} A^n_{\mathbf{k}} \; \hat{e} \cdot \mathbf{k} \propto (E^m_{\mathrm{b,exc}} - E^n_{\mathrm{b,exc}}) \int d\mathbf{r} F^{m*}(r) \hat{e} \cdot \mathbf{r} F^n(r)$, which yields the typical hydrogen like selection rules $\Delta l = \pm 1$, with l the angular momentum quantum number.

For the calculations on the MoS_2 polaritons we used an excitonic effective mass of 0.27

a.u. which is calculated from the G_0W_0 band structure. The Keldysh screened electron-hole interaction is calculated with a polarizability $\alpha = 13.5$a.u.. A comparison of exciton binding energies obtained with the MW model and from the solution of the BSE is shown in Fig. S4. With the MW we are then able to calculate all the excitonic quantities required in

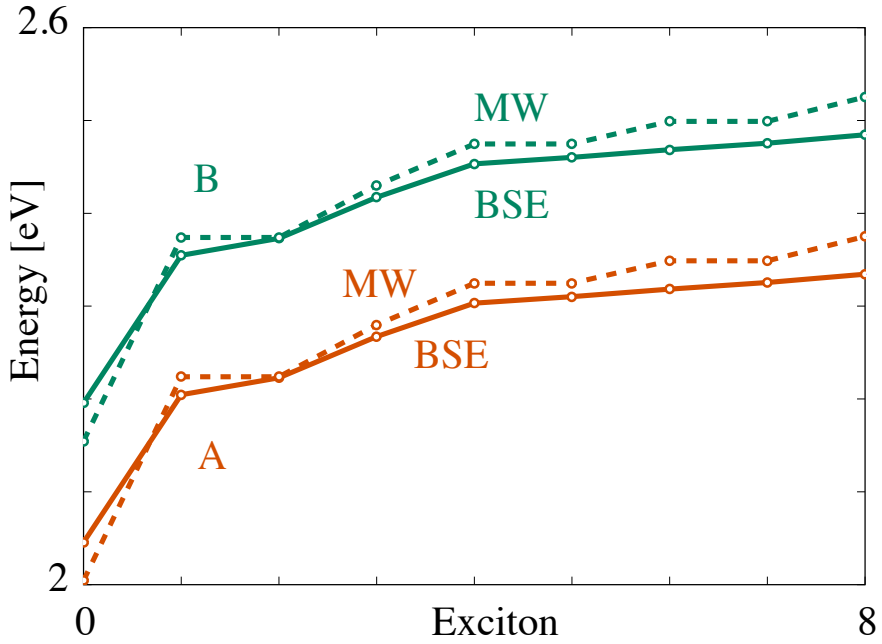

Figure S4: Comparison of excitons energies calculated using BSE and the Mott-Wannier (MW) model.

Eq. (2) of the main text and the same diagonalization procedure adopted in the QED-BSE can be performed to get the polaritonic states. Fig. S5 shows a side-by-side comparison of the polariton dispersion of MoS_2 obtained with the full QED-BSE approach and the QED-MW model. Small differences are apparent, that can be traced back to minor shifts in the exciton eigenvalues within the MW model, cf. Fig. S4 and differences in the momentum matrix elements. For a more detailed comparison, in Tab. S2 we reported values of the Rabi splittings and intensities of the response function for the "1s" A and "2s" A excitons within the QED-MW and QED-BSE methods.

We stress again that in the QED-MW, the exciton-polariton dispersion is now obtained at a much lower computational cost than for the QED-BSE case and at the same time a better

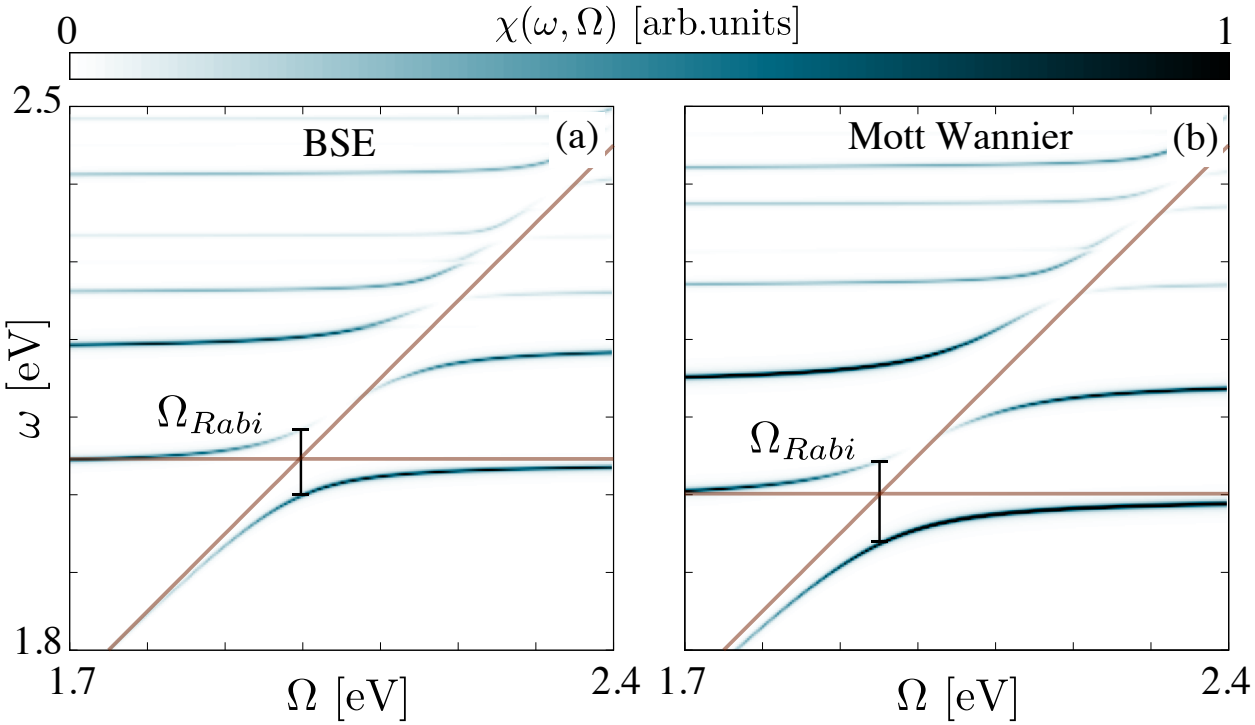

Figure S5: Comparison of QED-BSE and QED-MW for MoS_2 and with a coupling strength of $\tilde{A}_0 = 0.05$ a.u.

Table S2: QED-MW and QED-BSE comparison of Rabi splittings and response intensities for the 1s and 2s A excitons in MoS_2. The Rabi splitting are evaluated at the listed frequency Ω and the intensities are reported for the lower (LP) and upper (UP) polaritons with compatible arb.units.

Excitation	Ω (eV)	Rabi Splitting (eV)	χ_{LP} (arb.units)	χ_{UP} (arb.units)
		BSE		
1s A	2.00	0.084	21.33	1.19
2s A	2.16	0.041	0.75	7.45
		MW		
1s A	1.95	0.106	31.39	2.94
2s A	2.17	0.043	0.55	9.58

intuition on the photon mediated mixing of excitons can be built in terms of hydrogenic-like selection rules, according to Eqs. (5)-(9).

In the main text we used the MW model to access excitons in more complex materials, without increase in computational cost. In particular we studied the exciton-polariton dispersion in an MoS2 monolayer encapsulated in semi-infinite dielectric with a dielectric constant κ . For this particular stacking of materials, one can readily extend the QED-MW

for monolayers by including the effect of dielectric screening of the encapsulating material at three different levels: (i) the screened electron-hole Coulomb interaction is modified to[5]

$$W(\mathbf{r},\kappa) = \frac{1}{4\alpha}\left[H_0(\kappa x) - N_0(\kappa x)\right]_{x=r/2\pi\alpha} \tag{10}$$

(ii) the bare photon dispersion in the dielectric medium changes to $\omega = \omega_c/\sqrt{(}\kappa)$ and (iii) the effective vector potential amplitude becomes $A_0 \to A_0/\kappa$.[6] The extra electronic screening due to the dielectric not only modifies the exciton binding energies but it also renormalizes the electronic gap. To estimate the electronic band gap variation as a function of κ, we take the standard assumption[7] that the change in the binding energy of the $1s$ exciton compensates the renormalization of the band gap, hence the condition $E^{1s}_{\rm exc}(\kappa) = E^{1s}_{\rm exc}(\kappa = 0)$ must hold. The results are shown in the main text in Fig. 4.

Interlayer Excitons: Computational Details

In order to achieve an accurate first-principles description of the excitonic resonances in the MoS_2-WS_2 vdWH, we used the MW exciton model combined with the quantum electrostatic heterostructure (QEH) method in ref.[8] This method allows to account for dielectric screening effects on exciton binding energies and electronic band edges from ab-initio without restriction on lattice parameter matching between the two layers. We followed exactly the procedure used in ref.,[9] which for the sake of simplicity is summarized in the following. We first calculate GW band edges for each isolated monolayer and we then use the QEH-GW to include the effect of the dielectric screening induced by the adjacent layer and correct the electronic band edges position and band gap. In order to get the correct type II band alignment when compared to experiments,[10] norm-conserving PAW-setups are required.[11] We find a gap renormalization of ~ 0.132 eV for MoS_2 and ~ 0.137 eV for WS_2. Within the QEH we are then also able to calculate the screened interaction appearing in the MW model and calculate both interlayer and intralayer exciton binding energies. We find an interlayer

exciton binding energy of 0.28 eV and intralayer binding energy of 0.42 eV and 0.38 eV for MoS_2 and WS_2 respectively.

References

(1) Mortensen, J. J.; Hansen, L. B.; Jacobsen, K. W. *Phys. Rev. B* **2005**, *71*, 035109.

(2) Enkovaara, J.; Rostgaard, C.; Mortensen, J. J.; Chen, J.; Dułak, M.; Ferrighi, L.; Gavnholt, J.; Glinsvad, C.; Haikola, V.; Hansen, H. A. et al. *J. Phys.: Cond. Mat.* **2010**, *22*, 253202.

(3) Haastrup, S.; Strange, M.; Pandey, M.; Deilmann, T.; Schmidt, P. S.; Hinsche, N. F.; Gjerding, M. N.; Torelli, D.; Larsen, P. M.; Riis-Jensen, A. C. et al. *2D Mater.* **2018**, *5*, 042002.

(4) Latini, S.; Olsen, T.; Thygesen, K. S. *Phys. Rev. B* **2015**, *92*, 245123.

(5) Massicotte, M.; Vialla, F.; Schmidt, P.; Lundeberg, M. B.; Latini, S.; Haastrup, S.; Danovich, M.; Davydovskaya, D.; Watanabe, K.; Taniguchi, T. et al. *Nat. Commun.* **2018**, *9*, 1633.

(6) Grosso, G.; Parravicini, G. *Solid State Physics*; Elsevier Science, 2000.

(7) Ugeda, M. M.; Bradley, A. J.; Shi, S.-F.; da Jornada, F. H.; Zhang, Y.; Qiu, D. Y.; Ruan, W.; Mo, S.-K.; Hussain, Z.; Shen, Z.-X. et al. *Nat. Mater.* **2014**, *13*, 1091.

(8) Andersen, K.; Latini, S.; Thygesen, K. S. *Nano Lett.* **2015**, *15*, 4616–4621.

(9) Latini, S.; Winther, K. T.; Olsen, T.; Thygesen, K. S. *Nano letters* **2017**, *17*, 938–945.

(10) Heo, H.; Sung, J. H.; Jin, G.; Ahn, J.-H.; Kim, K.; Lee, M.-J.; Cha, S.; Choi, H.; Jo, M.-H. *Advanced Materials* **2015**, *27*, 3803–3810.

(11) Klimeš, J.; Kaltak, M.; Kresse, G. *Physical Review B* **2014**, *90*, 075125.